Nuclear Engineering and Technology 51 (2019) 573–578

Contents lists available at ScienceDirect

Nuclear Engineering and Technology

journal homepage: www.elsevier.com/locate/net

Original Article

Two-way fluid-structure interaction simulation for steady-state vibration of a slender rod using URANS and LES turbulence models

Tooraj Nazari [a], Ataollah Rabiee [a, *], Hossein Kazeminejad [b]

[a] Department of Nuclear Engineering, School of Mechanical Engineering, Shiraz University, 71936-16548 Shiraz, Iran
[b] Research School of Radiation Applications, Nuclear Science and Technology Research Institute, P. O. Box 11365-3486, Tehran, Islamic Republic of Iran

ARTICLE INFO

Article history:
Received 5 July 2018
Received in revised form
7 August 2018
Accepted 12 October 2018
Available online 12 October 2018

Keywords:
Flow-induced vibration
Fluid-structure interaction
URANS
LES
Steady state vibration
Viscous sub-layer

ABSTRACT

Anisotropic distribution of the turbulent kinetic energy and the near-field excitations are the main causes of the steady state Flow-Induced Vibration (FIV) which could lead to fretting wear damage in vertically arranged supported slender rods. In this article, a combined Computational Fluid Dynamics (CFD) and Computational Structural Mechanic (CSM) approach named two-way Fluid-Structure Interaction (FSI) is used to investigate the modal characteristics of a typical rod's vibration. Performance of an Unsteady Reynolds-Average Navier-Stokes (URANS) and Large Eddy Simulation (LES) turbulence models on asymmetric fluctuations of the flow field are investigated. Using the LES turbulence model, any large deformation damps into a weak oscillation which remains in the system. However, it is challenging to use LES in two-way FSI problems from fluid domain discretization point of view which is investigated in this article as the innovation. It is concluded that the near-wall meshes whiten the viscous sub-layer is of great importance to estimate the Root Mean Square (RMS) of FIV amplitude correctly as a significant fretting wear parameter otherwise it merely computes the frequency of FIV.

1. Introduction

In many industries, bundles of supported slender rods are the most crucial part of the design, such as heat exchangers, steam generators, power reactors, etc. In these components a fluid flow with high velocity is in touch with them; therefore, as highly energized fluid contacts these relatively flexible structures, fluid energy is absorbed by the elastic structures and so-called flow-induced vibration occurs [1]. Slender rods are often subjected to axial flow with high Reynold numbers and vibration of the rods takes place due to their exposure to flow turbulent forces, i.e. pressure field including far-field and near-field components. Far-field excitation is the propagating part of the disturbance and contributes in the form of acoustic. In contrary, near-field disturbance mainly originates from turbulent velocity fluctuations beneath Turbulent Boundary Layer (TBL). In short, it can be said that the pressure field always exists independent of structural movement which is random and asymmetric intrinsically [2,3].

Many efforts have been made to analytically and numerically investigate FSI of slender structures subjected to axial turbulent flow, which is studied in this paper. A very comprehensive discussion on analytical approaches can be found in Refs. [4,5]. However, CFD is widely being used to calculate wall-pressure spectra recently. Lee et al. [6] introduced a method based on time-mean flow fields predicted by RANS simulation in which pressure fluctuations can be solved using spectral correlation model using Green's function. The pressure field can be directly calculated using both Scale-Resolving Simulation (SRS) and Direct Numerical Simulation (DNS) which are very time-consuming and computationally too expensive [7–9]. The use of the LES turbulence model to predict the pressure filed have shown very promising results [10,11]. Application of URANS turbulence models is recently taken into consideration using combined CSM and CFD approach such as in Refs. [12,13] and application of LES in two-way FSI problems has been implemented such as in Refs. [14–16].

To the best of authors' knowledge, there is a few and incomprehensible information about two-way FSI problems with fully coupled CSM and CFD procedure considering the near-field effect, i.e. asymmetric turbulent boundary layer, which is the main source that keeps FIV in steady state. Moreover, authors' couldn't find any clear information about the required fluid mesh grid specification, which is discussed in the present study in detail as the innovation.

This paper is organized as follows. Section 2, discusses that the

* Corresponding author.
E-mail address: rabiee@shirazu.ac.ir (A. Rabiee).

https://doi.org/10.1016/j.net.2018.10.011

LES turbulence model performs well to compute asymmetric TBL parameters. Section 3, presents two-way FSI simulations for a single rod exposed to axial flow using an ordinary URANS turbulence model and concludes that such models are adequate to predict the modal characteristics including natural frequency and damping ratio. Section 4, re-simulates the single rod problem using the LES turbulence model in order to compute the exact amplitude of FIV as the novelty of this article. Section 5 concludes this paper.

2. LES analysis of Hooper's geometry

2.1. Filtered Navier-Stokes equations

Basically, LES computes the large scale eddies exactly and models the smallest eddies based on filtering i.e. scales smaller than the mesh size are filtered from the others [17]. In this section, thin turbulent boundary layer flow parallel to slender rods is solved numerically by means of LES with Kinetic Energy Transport Model (KETM) Sub-Grid Scale (SGS) model. Also, the described Dynamic Smagorinsky-Lilly Mode (DSM) is used in section 4.

The filtered Navier-Stokes governing equations for an incompressible fluid is as follows:

$$\frac{\partial \rho}{\partial t}+\frac{\partial}{\partial x_j}(\rho \overline{u}_i)=0 \tag{1}$$

$$\frac{\partial}{\partial t}(\rho \overline{u}_i)+\frac{\partial}{\partial x_j}(\rho \overline{u}_i \overline{u}_j)=-\frac{\partial \overline{p}}{\partial x_i}+\frac{\partial}{\partial x_j}\left(\mu \frac{\partial \overline{u}_i}{\partial x_j}\right)-\frac{\partial \tau_{ij}}{\partial x_j} \tag{2}$$

In these equations, ρ is the fluid density, $\overline{u}_i$ is the velocity of the fluid, $\overline{p}$ is the pressure and μ is the dynamic viscosity of the fluid. The last two terms on the right-hand side of the second equation are gradients of filtered laminar (molecular) shear stress and modelled turbulent (sub-grid scale) shear stress, respectively. It is noted that in this notation the filtered variables are denoted by an overbar. The effect of unresolved Kolmogorov scales appear in the SGS stress tensor which is modelled based on Boussinesq eddy viscosity approximation as follow:

$$\tau_{ij}-\frac{1}{3}\tau_{kk}\delta_{ij}=-2\mu_t \overline{S}_{ij} \tag{3}$$

where δ_{ij} is Kronecker delta, μ_t is the SGS turbulent viscosity and $\overline{S}_{ij}$ is the rate of resolved strain tensor defined as:

$$\overline{S}_{ij}\equiv\frac{1}{2}\left(\frac{\partial \overline{u}_i}{\partial x_j}+\frac{\partial \overline{u}_j}{\partial x_i}\right) \tag{4}$$

A detailed discussion on different SGS models can be found in Ref. [18].

2.2. Computational domain and solution procedure

As shown in Fig. 1, the test section resembles the square-pitch subchannel between six rods with the length of 9.14 m, set in a square-pitch array in order to investigate the fluid mechanics of an interior flow region inside a large infinite array of rods and taken from the experimental test of Hooper and Rehme [2]. No spacer grids or pins were used to omit any likely wake. Air was blown into the test section at a mean velocity of 10.3 m/s.

The limited area to the mid-rods and the red lines is the computational domain of interest with the length of 1.272 m, as used by the previous study of Chandra et al. [19]. The boundary conditions include velocity inlet for the inlet plane, no-slip

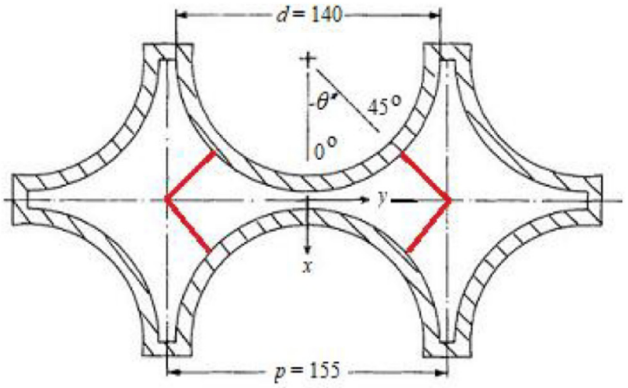

Fig. 1. The symmetrical square-pitch rod-cluster test section.

conditions for the rod walls, rotationally periodic for the top and bottom side boundaries of the fluid domain to produce the geometry of an infinite array of rods and pressure outlet for the outlet plane.

In LES analysis the dimensionless wall distance, y^+, must be payed attention carefully. In well resolved LES $y^+\approx 1$ and can be greater at high Reynold numbers if accuracy is not crucial near the wall region. The computational domain contains 2,280,000 cells and the grid is carefully stretched both in the streamwise and the spanwise directions. The grid has 3 cells within the viscous sublayer, i.e. $y^+\leq 5$ with the first point located at $y^+\approx 1$ and the radial grid growth rate is 1.05.

The two key criteria for any LES analysis are the grid size and the time step. The larger scale, l, is proportional to one-tenth of the boundary layer thickness, δ. The Kolmogorov microscale, η, is related to a larger scale by equation $l\sim\eta Re_t^{3/4}$ and $\eta\equiv(\nu^3/\varepsilon)^{1/4}$ where ν and ε are the kinematic viscosity of the fluid and the average rate of dissipation of turbulence kinetic energy per unit mass, respectively. Another important length scale related to LES from the statistical theory of turbulence is Taylor microscale, $\lambda\sim\sqrt{10}\eta^{2/3}l^{1/3}$. The grid filter width must lie between Taylor and Kolmogorov microscales as is shown in Fig. 2. Similarly, the time step must lie between Taylor time scale ($\lambda_t=(15\nu/\varepsilon)^{1/2}$) and Kolmogorov time scale ($\tau\equiv(\nu/\varepsilon)^{1/2}$) which is selected 0.00035 s [17].

Results of the axial velocity component at mid-length of the domain at points $(0,\mp 0.0102,0.636)$ m, are given in Fig. 3. The experimental data reveals that the axial velocity fluctuations mostly vary within ±1.3 m/s which is about 15% of the bulk velocity

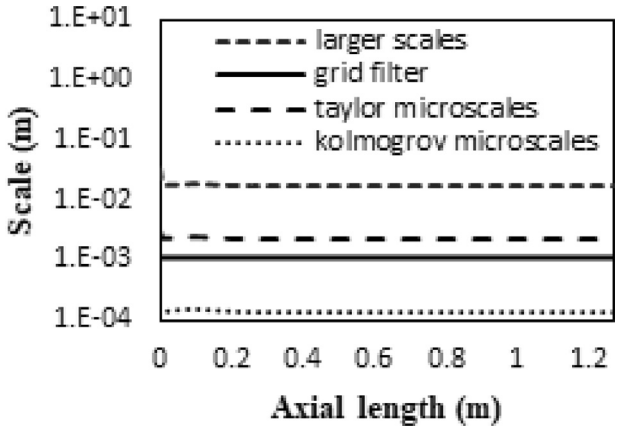

Fig. 2. Comparison of different scales along the line $\boldsymbol{x}=0,\boldsymbol{y}=0,\boldsymbol{z}$.

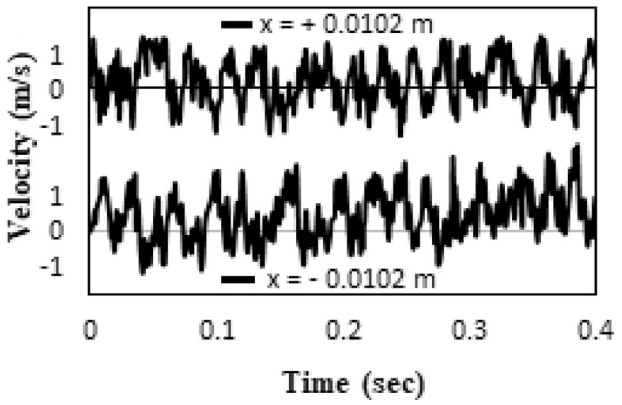

Fig. 3. Experimental axial velocity profiles [2].

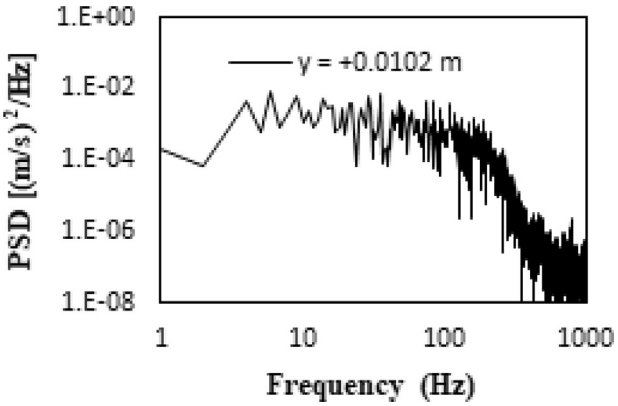

Fig. 6. PSD of velocity fluctuations at point (0, +0.0102, 0.636) m.

with an estimated error of 15% [20].

The notable feature is the uncorrelated relationship of the large-scale *u*-structure in the neighbouring subchannels as described in Hooper and Rehme [2]. Accordingly, the calculated axial velocity profiles from LES simulation at the same points are represented in Fig. 4. As can be seen, the velocity profiles are dissimilar and have an antiphase relationship in a periodic geometry which varies between ±1.5 m/s and are approximately in good agreement with experimental data based on 15% estimation error.

Power Spectral Densities (PSD) of the axial velocity fluctuations are shown in Figs. 5 and 6. The results depict there is a band of dominant frequencies below 100 Hz. In order to demonstrate that the loading is random on the rods surface, the computed results for the static pressure fluctuations normal to the rods at points $(\mp 0.0075,\ 0,\ 0.636\,m)$ are shown in Fig. 7, respectively. Similarly, the profiles of the static pressures has an antiphase relationship on transverse nodes in a periodic geometry the same as the axial velocity profiles.

From the computed parameters on the transverse points, it can be concluded that the turbulent boundary layer is asymmetric and energetic enough to produce random near-field excitations adjacent to the rods, which in turn are the main cause of FIV.

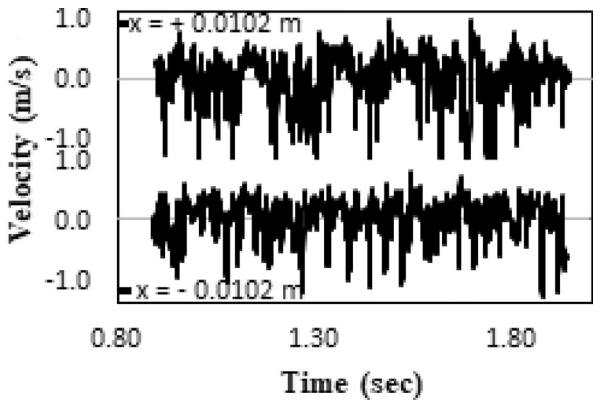

Fig. 4. Computed axial velocity profiles from LES simulation.

3. Two-way FSI simulation using a URANS model

3.1. Governing equations

Any FSI problem can be reformulated into three coupled sub-problems: (1) Fluid problem, (2) Structure problem and (3) Interfacial condition. The fluid and the structure domains are solved separately in a sequential manner with their individual grids and the interfacial conditions are used explicitly to communicate information between the fluid and structure solutions [21].

Overview of the FSI approach which is used in this research is as follows:

3.1.1. Fluid field simulation

The fluid domain is an unsteady incompressible turbulent flow field and is modelled using the Navier-Stokes (NS) equations. In Reynolds averaging [17], any variable is decomposed into the mean and fluctuating components, i.e. $\varphi = \overline{\varphi} + \varphi'$. Dropping the overbar

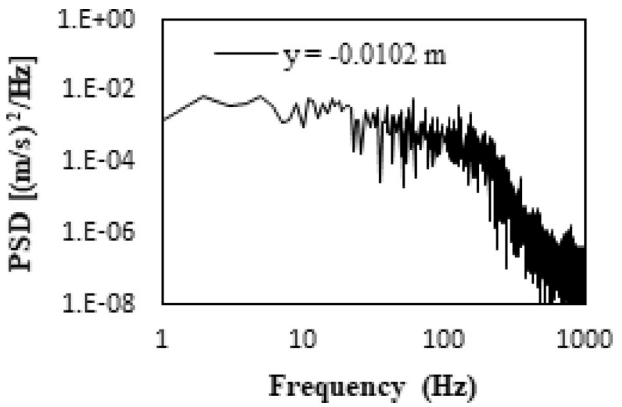

Fig. 5. PSD of velocity fluctuations at point (0, - 0.0102, 0.636) m.

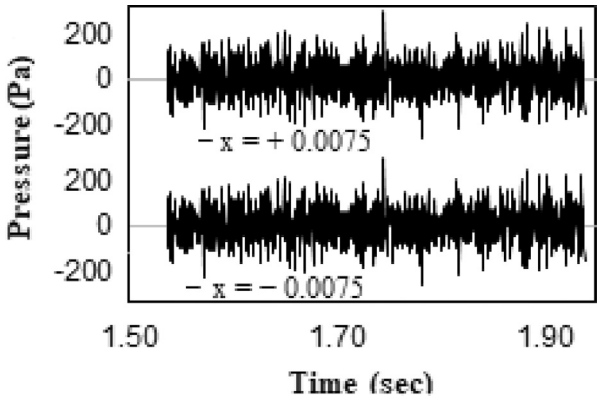

Fig. 7. Computed static pressure profiles from LES simulation.

on mean values for simplicity, URANS equations can be written as follow:

$$\frac{\partial \rho^f}{\partial t} + \frac{\partial}{\partial x_j}\left(\rho^f u_i^f\right) = 0 \tag{5}$$

$$\frac{\partial}{\partial t}\left(\rho u_i^f\right) + \frac{\partial}{\partial x_j}\left(\rho u_i^f u_j^f\right) = f_i^f + \frac{\partial}{\partial x_j}\left[-p^f\delta_{ij} + \mu\left(\frac{\partial u_i^f}{\partial x_j} + \frac{\partial u_j^f}{\partial x_i} - \frac{2}{3}\delta_{ij}\frac{\partial u_i^f}{\partial x_i}\right) - \rho\overline{u_i'^f u_j'^f}\right] \tag{6}$$

where x_i (i = 1,2,3) are Cartesian coordinates and ρ^f, u_i^f, f_i^f, p^f, μ denote the fluid density, the fluid velocity, the fluid body force, the fluid pressure and the fluid dynamic viscosity, respectively. The terms in the bracket make the fluid stress tensor and the last term in the bracket is the Reynolds stresses that represents turbulence effect and must be modelled. In this regard, the shear-stress transport (SST) k-ω model is used [17].

3.1.2. Structural domain simulation

The governing equation of an elastic solid is as follow:

$$\rho^s\frac{\partial u^s}{\partial t} = \mathrm{f}^s + \nabla.\sigma \tag{7}$$

where ρ^s, f^s, u^s, σ denote the solid density, the body force, the solid velocity and the solid stress tensor, respectively.

3.1.3. The interfacial constraints

Both the kinematics and the dynamic constraints must be met on the interface. The kinematic constraint requires that the structure velocity be equals to the fluid velocity, whereas the dynamic constraint requires that the stress tensors of the structure and the fluid normal to the interface be equal. These constraints can be written as:

$$u_i^s - u_i^f = 0 \tag{8}$$

$$\sigma_{ij}^s n_j - \sigma_{ij}^f n_j = 0 \tag{9}$$

where n_j is the component of the normal vector at the interface.

The FSI simulations are performed by means of ANSYS software, in which the fluid domain is solved using Fluent and the structural domain is solved using the Mechanical module. Meanwhile, data transferring process is performed by System coupling.

3.2. Description of the problem

The problem of interest is taken from the experimental test of Chen and Wambsganss [3] and involves a brass rod with a diameter of 0.0127 m and length of 1.19 m which is clamped at both ends and exposed to a turbulent annular flow within a cylindrical channel with a diameter of 0.0254 m.

To demonstrate the effect of the flow velocity on modal characteristics of the rod due to FSI, three inlet flow velocities are chosen including 10 m/s, 20 m/s and 30 m/s. The water density is 1000 kg/m^3 and the dynamic viscosity of the water is 0.001 Pa.s. The turbulence intensity and the length scale at the entrance of the fluid domain are 5% and 0.001 m, respectively.

The applied fluid domain mesh consists of 6 radial, 20 circumferential and 250 axial divisions. The structure domain mesh consists of 11 cross-sectional cells and 250 axial divisions. The FSI simulations were performed with a time step of 5.0e-4 s. Moreover, on the FSI case with a flow velocity of 10 m/s, the mesh sensitivity analysis with a doubled number of divisions and the time step of 2.5e-4 s were performed which revealed that the results are both independent of mesh size and time step. The lateral displacement of the rod in the y-direction at $x = l/2$ is shown in Fig. 8.

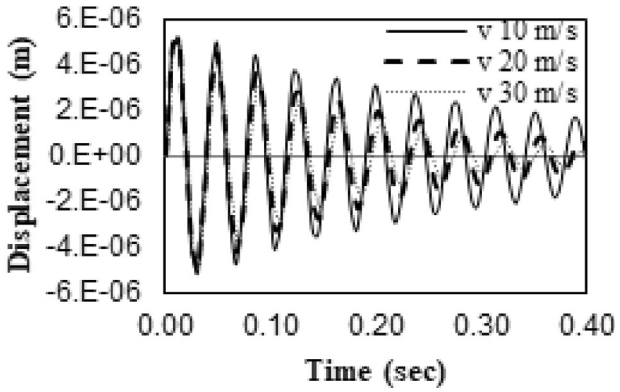

Fig. 8. Rod displacement at $x = l/2$ (SST k-ω).

Table 1 lists the measured and the calculated values of the rod's modal characteristics. The fundamental frequency decreases due to the effect of added mass and may increase or decrease with flow velocity depending on the end conditions [3] and the result of these factors determine the frequency of the system. As expected the computed natural frequency (f) decreases with the increasing flow velocity whereas, the damping ratio (ξ) increases linearly with the increasing the flow velocity which is due to increased drag force [3] and the results are in good agreement with the experimental values.

In the next section, this problem using the LES turbulence model is re-simulated.

4. Two-way FSI simulation using LES model

The governing equations of the problem are already discussed in sections 2.1 and 3.1 in detail. In order to solve the fluid field via the LES model, much more mesh is required rather than the ordinary URANS models.

In our problem of interest, the annular flow may be regarded as a flow between parallel flat plates which have been wrapped around their concentric axis. Then, the turbulent boundary layer thickness, δ, for $Re_x \geq 3 \times 10^6$ can be estimated by

$$\delta = 0.37x/Re_x^{0.2} \tag{10}$$

$$Re_x = \frac{U_0 x}{\nu} \tag{11}$$

where U_0, x and ν are the fluid velocity, the distance from the front

Table 1
Experimental and computed values of f and ξ for the fundamental mode.

Water Velocity (m/s)	10	20	30
Natural frequency (Hz)			
- Experiment [3]	27.9	27.7	27.5
- Computed	26.9	26.8	26.6
Damping ratio			
- Experiment	0.013	0.021	0.030
- Computed	0.012	0.020	0.029

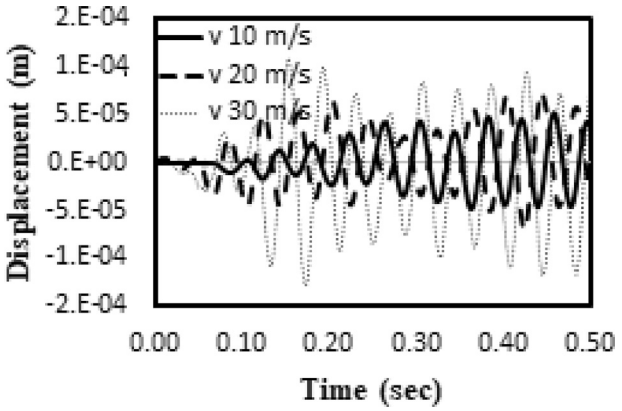

Fig. 9. Rod displacement at $x = l/2$ (LES).

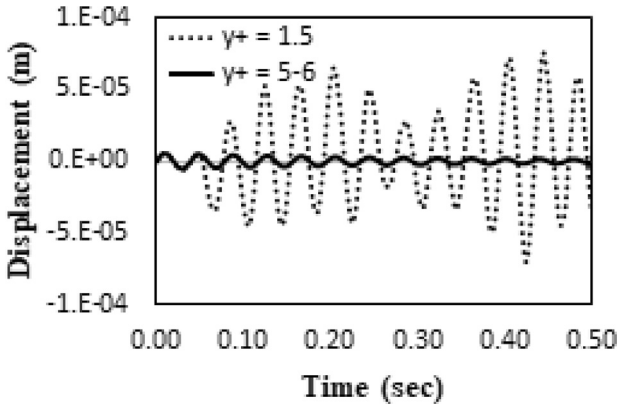

Fig. 11. Mid-rod displacement (V = 20 m/s, LES).

Table 2
Measured and calculated RMS of FIVs.

Velocity (m/s)	10	20	30
RMS of FIV (m)			
- Measured	5.0e-5	7.0e-5	1.0e-4
- Computed	4.32e-5	6.82e-5	0.91e-4
- Error (%)	13.6	2.6	9.0

edge and the fluid kinematic viscosity, respectively [22].

The value of Re_x for the flow velocities of 10, 20 and 30 m/s, rod length of 1.19 m and the fluid kinematic viscosity of 1.0e-6 m^2/s are 11.9e6, 23.8e6 and 35.37e6 which give the thickness of TBLs 0.0169, 0.0147 and 0.0135 m, respectively. Accordingly, the ratio of the TBLs' thickness to the rod's radius are greater than one which suggests that the flow is fully developed through the channel and the entrance length is very short. Therefore, the domain of the fluid flow cannot be divided into a thin TBL and a thick mainstream domains, therefore, the whole domain of the fluid must be meshed appropriately. However, such a mesh results in an excessive computational cost and to avoid that, the fluid domain near the inner wall was meshed finer than the rest of the domain. This means that $y^+ \approx 1$ and the near-wall grid filter width equals to the Kolmogorov microscale and meshes are stretched finely until the grid filter width equals to Taylor microscale and then it was kept constant. Taking into account the criteria mentioned section 2, the time step was selected 0.5 ms.

The displacements of the mid-rod in y-direction are shown in Fig. 9 and Table 2 lists the experimental and the calculated values of RMS of FIVs.

The calculated frequencies for all the cases are about 27.3 Hz with the difference in the second decimal place which are consistent with the calculated values in the previous section and the experimental values with 0.25 Hz uncertainty. It also revealed that the vibration amplitude increases with increasing fluid velocity.

4.1. Grid study

LES is a grid-dependent technique, therefore, coarser grids are also used and compared with the finer grids' results. The y-direction displacement of the rod at $x = l/2$ for the case with the fluid velocity of 10 m/s is shown in Fig. 10. It reveals that the amplitude of the rod displacement is under-predicted by the coarser grid with $y^+ = 6.5$ and the RMS value of the displacement is 1.96e-5 m which is far less than both the experimental and the computed values from the finer grid with $y^+ \approx 1$. Figs. 11 and 12 represent the y-direction displacement of the rod at $x = l/2$ for the cases with the fluid velocities of 20 and 30 m/s respectively. As can be seen, the vibrations has steady state response; however, the amplitude of the displacements are under-predicted. The reason for this will be discussed in the next section.

4.2. Model verification

The LES index of quality (*LES IQ*) proposed by Ref. [23] is a quality assessment measure to show a good verification of SGS simulation. It is useful to express *LES IQ* as the ratio of the resolved turbulent kinetic energy (k^{res}) to the total turbulent kinetic energy (k^{tot}) so the

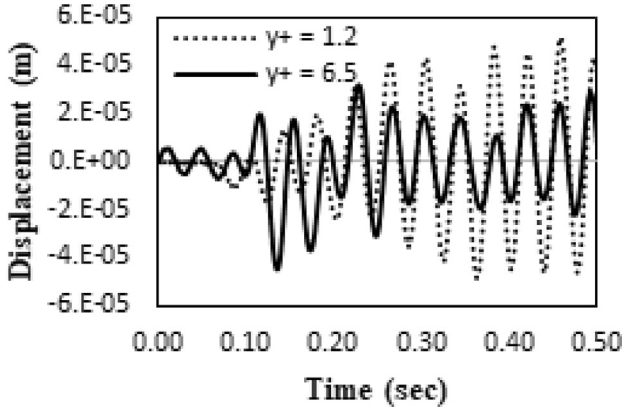

Fig. 10. Mid-rod displacement (V = 10 m/s, LES).

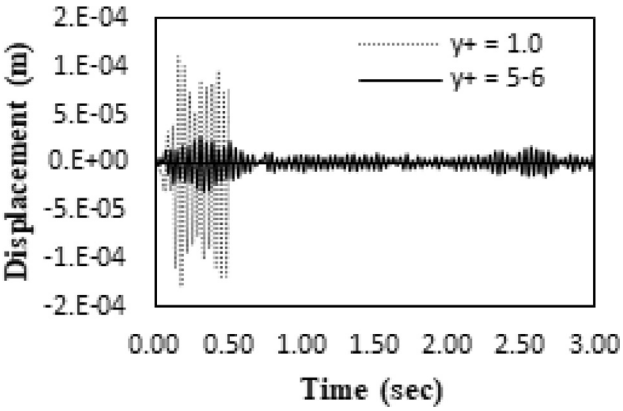

Fig. 12. Mid-rod displacement (V = 30 m/s, LES).

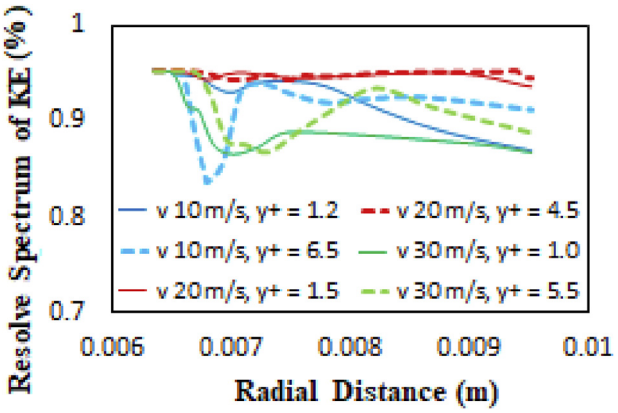

Fig. 13. *LES IQ* across the boundary layer.

index of quality is a number between 0 and 1. For most engineering applications at high *Re* numbers, $IQ \geq 0.75$ is enough; however, it has been shown that in some engineering applications $IQ = 0.65$ works well and the index of quality above 0.8 is strict [18].

Fig. 13 compares *LES IQ* for the flow velocities of 10, 20 and 30 m/s across the boundary layer at mid-height of the rod along the line $r,\ \theta = 0^{\circ},\ z = 0.595\ m$ between the coarse and the fine grids of the fluid domain with the same structural grid.

The presented results show that over 80 percent of the kinetic energy has been resolved, however when the first mesh point is out of the viscous sub-layer, the RMS of FIV amplitudes are under-predicted which suggests the importance of viscous sub-layer and that viscous shears are not negligible. The viscous forces dominate over inertial forces within the viscous sub-layer and it is necessary to be accurately computed, and this becomes more intense as the Reynolds number increases.

5. Conclusion

Pressure excitation is the main reason for the steady state flow-induced vibration of the supported rods which could lead to fretting wear damage in the long term. In this study, using the LES turbulence model it is shown that the random pressure field around vertically arranged rods always exists independent of the fluid-structure interaction and LES performs well in predicting the asymmetric random pressure field adjacent to the rods. Both the URANS (SST k-ω) and the LES turbulence models computed the modal characteristics of a vibrating brass rod exposed to axial flow effectively. It is revealed that in two-way FSI simulations, the amplitude of the vibration increases with upstream fluid flow velocity although, the computed frequencies are approximately constant about 27 Hz and are in close agreement with the experimental data. However, to use LES in two-way FSI problems certain fluid grid specifications must be met. The mesh size near the wall must be equal to the order of Kolmogorov scales and be stretched carefully, nevertheless the size of the largest mesh should not be larger than the Taylor microscales. It is shown that if the parameter of interest is the amplitude of FIV, the viscous forces are not negligible and at least some mesh points must locate within the viscous sub-layer to resolve viscous shears correctly.

Appendix A. Supplementary data

Supplementary data to this article can be found online at https://doi.org/10.1016/j.net.2018.10.011.

References

[1] R.D. Blevins, Flow-induced vibration in nuclear reactors: a review, Prog. Nucl. Energy 4 (1979) 25–49, https://doi.org/10.1016/0149-1970(79)90008-8.
[2] J.D. Hooper, K. Rehme, Large-scale structural effects in developed turbulent flow through closely-spaced rod arrays, J. Fluid Mech. 145 (1984) 305, https://doi.org/10.1017/S0022112084002949.
[3] S. Chen, M.W. Wambsganss, Parallel-flow-induced vibration of fuel rods, Nucl. Eng. Des. 18 (1972) 253–278.
[4] M.P. Paidoussis, Fluid-structure Interactions: Slender Structures and Axial Flow, Academic press, 1998.
[5] M.P. Paidoussis, Fluid-structure Interactions: Slender Structures and Axial Flow, Academic press, 2004.
[6] Y.-T. Lee, W.K. Blake, T.M. Farabee, Modeling of wall pressure fluctuations based on time mean flow field, J. Fluid Eng. 127 (2005) 233–240, https://doi.org/10.1115/1.1881698.
[7] F. Abbasian, S.D. Yu, J. Cao, Experimental and numerical investigations of three-dimensional turbulent flow of water surrounding a CANDU simulation fuel bundle structure inside a channel, Nucl. Eng. Des. 239 (2009) 2224–2235, https://doi.org/10.1016/j.nucengdes.2009.06.012.
[8] M.A. Christon, R. Lu, J. Bakosi, B.T. Nadiga, Z. Karoutas, M. Berndt, Large-eddy simulation, fuel rod vibration and grid-to-rod fretting in pressurized water reactors, J. Comput. Phys. 322 (2016) 142–161, https://doi.org/10.1016/j.jcp.2016.06.042.
[9] A.M. Elmahdi, R. Lu, M.E. Conner, Z. Karoutas, E. Baglietto, Flow induced vibration forces on a fuel rod by les cfd analysis, in: Proc. NURETH14 Conf. Toronto, Ontario, Canada, 2011.
[10] B. Konig, E. Fares, M.R. Khorrami, P.A. Ravetta, A comparative study of simulated and measured main landing gear noise for large civil transports, in: 23rd AIAA/CEAS Aeroacoustics Conf, 2017, p. 3013.
[11] J. De Ridder, J. Degroote, K. Van Tichelen, P. Schuurmans, J. Vierendeels, Predicting turbulence-induced vibration in axial annular flow by means of large-eddy simulations, J. Fluid Struct. 61 (2016) 115–131, https://doi.org/10.1016/j.jfluidstructs.2015.10.011.
[12] D. De Santis, A. Shams, Numerical modeling of flow induced vibration of nuclear fuel rods, Nucl. Eng. Des. 320 (2017) 44–56, https://doi.org/10.1016/j.nucengdes.2017.05.013.
[13] E. ter Hofstede, S. Kottapalli, A. Shams, Numerical prediction of flow induced vibrations in nuclear reactor applications, Nucl. Eng. Des. 319 (2017) 81–90, https://doi.org/10.1016/j.nucengdes.2017.04.026.
[14] Z.G. Liu, Y. Liu, J. Lu, Numerical simulation of the fluid-structure interaction for two simple fuel assemblies, Nucl. Eng. Des. 258 (2013) 1–12, https://doi.org/10.1016/j.nucengdes.2013.01.029.
[15] H. Yuan, J. Solberg, E. Merzari, A. Kraus, I. Grindeanu, Flow-induced vibration analysis of a helical coil steam generator experiment using large eddy simulation, Nucl. Eng. Des. 322 (2017) 547–562, https://doi.org/10.1016/j.nucengdes.2017.07.029.
[16] X. Zhang, Numerical and Experimental Investigations on Vibration of Simulated CANDU Fuel Bundles Subjected to Turbulent Fluid Flow, 2011.
[17] D.C. Wilcox, Turbulence Modeling for CFD, DCW industries La Canada, CA, 1998.
[18] N. Baghernezhad, O. Abouali, Different SGS models in large eddy simulation of 90° square cross-section bends, J. Turbul. 11 (2010) N50, https://doi.org/10.1080/14685248.2010.520016.
[19] L. Chandra, F. Roelofs, E.M.J. Komen, E. Baglietto, Unsteady RANS and LES analyses of hooper s hydraulics experiment in a tight lattice bare rod-bundle, in: 8th Int. Top. Meet. Nucl. Therm. Oper. Saf. (NUTHOS-8), Shanghai, 2010, pp. 1–13.
[20] S.V. Möller, On phenomena of turbulent flow through rod bundles, Exp. Therm. Fluid Sci. 4 (1991) 25–35, https://doi.org/10.1016/0894-1777(91)90018-M.
[21] G. Hou, J. Wang, A. Layton, Numerical methods for fluid-structure interaction — a review, Commun. Comput. Phys. 12 (2012) 337–377, https://doi.org/10.4208/cicp.291210.290411s.
[22] B.R. Munson, D.F. Young, T.H. Okiishi, Fundamentals of Fluid Mechanics, 1990, p. 3. New York.
[23] I.B. Celik, Z.N. Cehreli, I. Yavuz, Index of resolution quality for large eddy simulations, J. Fluid Eng. 127 (2005) 949–958.